

# Thermodynamic stability of oxygen point defects in cubic Zirconia

Amit Samanta\*

<sup>1</sup>*Program in Applied and Computational Mathematics,  
Princeton University, Princeton, New Jersey 08544, USA*

Thomas Lenosky and Ju Li

<sup>2</sup>*Department of Materials Science and Engineering,  
University of Pennsylvania, Philadelphia, Pennsylvania 19103, USA*

(Dated: September 29, 2010)

## Abstract

Zirconia ( $\text{ZrO}_2$ ) is an important material with technological applications which are affected by point defect physics. Ab-initio calculations are performed to understand the structural and electronic properties of oxygen vacancies and interstitials in different charge states in cubic zirconia. We find oxygen interstitials in cubic  $\text{ZrO}_2$  can have five different configurations -  $\langle 110 \rangle$  dumbbell,  $\langle 100 \rangle$  dumbbell,  $\langle 100 \rangle$  crowd-ion, octahedral, and  $\langle 111 \rangle$  distorted dumbbell. For a neutral and singly charged oxygen interstitial, the lowest energy configuration is the  $\langle 110 \rangle$  dumbbell, while for a doubly charged oxygen interstitial the octahedral site is energetically the most favorable. Both the oxygen interstitial and the oxygen vacancy are negative- $U$ , so that the singly charged defects are unstable at any Fermi level. The thermodynamic stability of these defects are studied in terms of Fermi level, oxygen partial pressure and temperature. A method to determine the chemical potential of the system as a function of temperature and pressure is proposed.

## 1. Introduction

Zirconia ( $\text{ZrO}_2$ ) exists in three closely related phases with monoclinic, tetragonal and cubic symmetry. The monoclinic phase is thermodynamically stable near room temperature and up to 1400 K, while at higher temperatures tetragonal and then cubic phases become stable.<sup>1</sup> Cubic zirconia is stable above 2570 K.<sup>1</sup> However, the cubic phase can be stabilized at much lower temperatures by doping  $\text{ZrO}_2$  with divalent or trivalent cations like  $\text{Y}^{3+}$  or  $\text{Ca}^{2+}$ .<sup>2</sup> This cubic stabilized zirconia (CBZ) has high thermal shock resistance, high strength and toughness and has been under extensive investigation in recent years.<sup>2,3</sup> CBZ is also important for oxygen sensors and fuel cells.<sup>4-6</sup> To satisfy charge neutrality condition after cation doping, these materials contain oxygen vacancies and interstitials whose concentrations are related to the dopant concentration.

Unstabilized cubic zirconia is also an interesting material for high temperature applications. A proposed methodology for exterior coatings in high speed aircraft involves coating with  $\text{ZrB}_2/\text{SiC}$  ceramic.<sup>7,8</sup> Upon exposure to high temperatures in an oxidizing atmosphere,  $\text{ZrB}_2/\text{SiC}$  oxidizes to  $\text{ZrO}_2$  and  $\text{SiO}_2+\text{B}_2\text{O}_3$ , a vitreous borosilicate glass which forms a sticky layer on the top.<sup>9</sup> Little is known about point defects and their stability for the high temperature phase of  $\text{ZrO}_2$ , yet defect diffusion within the oxide scale is potentially a key issue for optimization of this material system, and experimental studies are difficult because of the extreme operating conditions.

Moreover, the semiconductor industry has recently begun using hafnia and zirconia as a substitute for silicon dioxide in MOSFET gate dielectrics, an application for which they have merit because of their high dielectric constant.<sup>10-12</sup> For this application the crystalline structure is generally the low-temperature monoclinic phase. Also CBZ has good resistance to radiation induced damage, leading to a number of proposed and actual nuclear applications.<sup>13-16</sup> For both of these applications point defect physics are crucial. In the gate oxide application point defects can trap and scatter charge carriers and create other unfavorable effects. In the nuclear applications the rapid recombination of radiation-induced defects gives zirconia its radiation resistance.

In this paper we study point defect formation in cubic  $\text{ZrO}_2$  by using first principles density functional theory calculations. First we obtain the atomic structure and formation energy of the different intrinsic defects. Then we present results in which we calculate defect concentrations as a function of Fermi level, oxygen partial pressure and temperature, by studying the thermodynamic equilibria for the various defects with each other, with ambient oxygen, and with charge carriers.

## 2. Method of calculation

We perform calculations using the Vienna Ab-Initio Simulation Package (VASP),<sup>17-19</sup> a plane wave basis density functional theory (DFT) code, with generalized gradient approximation (GGA) and the exchange correlation potential of Perdew, Burke and Wang (PBE).<sup>20</sup> Spin polarization is taken into account in these calculations. The wave functions are expanded to a plane wave cut-off of 520 eV. Static relaxations are performed till the forces on individual atoms are smaller than  $10^{-4}$  eV/Å and total energy convergence within  $10^{-5}$  eV is achieved. Initial  $\mathbf{k}$ -point sampling is performed with 1 to 20 irreducible  $\mathbf{k}$ points in the first Brillouin zone. The equilibrium lattice parameter of cubic ZrO<sub>2</sub> is 5.1276 Å (with 20 irreducible  $\mathbf{k}$ points) which is close to previous density functional calculations and experimental values.<sup>10,21</sup> All subsequent defect calculations are performed at this lattice constant, with no relaxation of the super cell unless otherwise mentioned. Total energy of a cubic ZrO<sub>2</sub> primitive cell converged to within 6 meV with 4 irreducible  $\mathbf{k}$ points. Hence, we use 4 irreducible points for all subsequent calculations.

The band gap is given by the energy difference between the highest occupied electronic energy level and the lowest unoccupied energy level. We obtain a band gap of 3.26 eV which is smaller than 5.40 eV obtained using GW calculations.<sup>10,12,22</sup> DFT calculations are known to underestimate the band gap.<sup>12</sup> To describe the DOS of the defect-free cell obtained from VASP calculations, a rigid shift of the conduction band edge is performed to obtain the experimentally reported band gap. The defect levels are not scaled while shifting the conduction band edge.<sup>10,12</sup>

Understanding the thermodynamic stability of charged defects involves incorporation or removal of electrons from the defect-free materials surrounding the defect. In the DFT calculations, the electronic charge neutrality of the supercell is achieved by a uniform jellium of equal and opposite charge. This results in long range interaction between the defect and its periodic images in the calculation which must be subtracted off from the total energy of the supercell  $E_{\text{vasp}}$ . Thus  $E = E_{\text{vasp}} - E_{\text{cor}}$  is the corrected energy of the system.  $E_{\text{vasp}}$  is the energy obtained from VASP calculations for a sample containing defects. For a single defect the correction term is<sup>23</sup>

$$E_{\text{cor}} = -\frac{q^2\alpha}{4\pi L\kappa\epsilon_0} \quad (1)$$

where  $q$  is the charge on the defect,  $\alpha = 5.04$  is the Madelung constant,  $L$  is the length of the cubic supercell used for calculations,  $\kappa$  is the dielectric constant of cubic ZrO<sub>2</sub> and  $\epsilon_0$  is the permittivity of free space. For cubic zirconia, we take  $\kappa = 36.8$ .<sup>1</sup> Typical Madelung corrections in our supercells are of the order of  $0.05q^2$  eV, where  $q$  is the charge of the defect ( $\dots, -2, -1, 0, 1, 2, \dots$ ).

Given our primary interest in the high temperature cubic phase we calculate formation free energies for the lattice defects in zirconia as a function of temperature and oxygen partial pressure.

### 3. Defect geometry, electronic charge state and stability

Stability of point defects have to be analyzed with respect to some reference state. Since cubic zirconia is a high temperature phase and frequently used in contact with atmosphere we use oxygen gas molecule as the reference state for calculations of formation energies of oxygen vacancies and oxygen interstitials.

#### 3A. Reference state calculations

First-principles calculations of an oxygen molecule are performed at  $T = 0$  K. The triplet state is found to be the ground state of  $O_2$ . We find  $E_{O_2}^{vasp} = -9.86$  eV and a bond length of 1.23 Å. The singlet state is 1.06 eV higher than the triplet state.

The chemical potential ( $\mu_{O_2}$ ) of an oxygen gas molecule changes with temperature as well as the oxygen partial pressure. An estimate of the free energy of an oxygen molecule can be made based upon the quantum formulation of an ideal gas. The free energy of an ideal diatomic gas has contributions from the translational free energy, vibrational free energy and rotational free energy.<sup>24</sup> So the chemical potential of an oxygen molecule as a function of temperature ( $T$ ) and pressure ( $P$ ) is given by :<sup>24</sup>

$$\mu = k_B T \log \left( \frac{P \lambda^3}{k_B T} \right) - k_B T \log \left( \frac{4\pi^2 I k_B T}{h^2} \right) + \frac{1}{2} \hbar \omega_o + k_B T \log \left[ 1 - \exp \left( -\frac{\hbar \omega_o}{k_B T} \right) \right] \quad (2)$$

where,  $\lambda$  is the thermal de-Broglie wavelength,  $k_B$  is the Boltzmann constant,  $h$  is Planck's constant and  $I$  is the moment of inertia of the oxygen molecule. The chemical potential can also be expressed in terms of a reference pressure  $P_r$ :

$$\mu = \mu_r + k_B T \log \frac{P}{P_r} \quad (3)$$

where,  $\mu_r$  is the chemical potential at reference pressure. The reference pressure is generally taken as 1 atm. From ab-initio calculations, we find the vibrational frequency of  $O_2$  is  $\omega_o = 1568.06$   $cm^{-1}$ , which is close to experimental result of  $\omega_o = 1565.4$   $cm^{-1}$ .<sup>25</sup> For our subsequent analysis, the chemical potential of an oxygen atom is taken as half of  $\mu_{O_2}$  :

$$\mu_O(T, P) = \frac{1}{2} \mu_{O_2}(T, P) \quad (4)$$

Fig. 1 shows the variation in the oxygen chemical potential with temperature at different oxygen partial pressures. From this analysis we obtain  $\mu_{\text{O}}(T = 300 \text{ K}, P = 1 \text{ atm}) = -5.16 \text{ eV}$  and  $\mu_{\text{O}}(T = 2600 \text{ K}, P = 1 \text{ atm}) = -8.20 \text{ eV}$ . Since, the cubic phase in undoped  $\text{ZrO}_2$  is stable above 2570 K, we have used  $T = 2600 \text{ K}$ , for subsequent analysis.

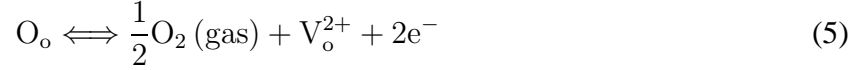
### 3B. Oxygen Vacancy

Oxygen vacancies in cubic  $\text{ZrO}_2$  have been discussed previously because their motion is related to the ionic conductivity of zirconia. They have also been studied to understand the defect levels, which are important for applications in the semiconductor industry.<sup>10,12</sup> In the low temperature monoclinic phase there are two non-equivalent oxygen lattice sites, and hence oxygen vacancies exhibit different coordination numbers.<sup>10</sup> In contrast, all oxygen vacancy sites in cubic zirconia are equivalent, and have four-fold coordination.

In accord with previous work, we find that point defects significantly distort the nearby lattice.<sup>26–28</sup> For different charge states the lattice relaxations around the vacancy are qualitatively different. Formation of neutral vacancy,  $V_{\text{O}}$  (using Kroger-Vink notation<sup>29</sup>) results in inward displacement of the nearest neighbors. Allowing the volume of supercell to relax results in decrease in total volume by  $1.03 \text{ \AA}^3$ . The neighboring Zr and oxygen ions move towards the oxygen vacancy. In contrast to  $V_{\text{O}}$ , the atomic structures of  $V_{\text{O}}^{1+}$  and  $V_{\text{O}}^{2+}$  have outward movement of Zr ions while the oxygen ions move inwards. With increase in charge on the vacancy we find increase in distortion of the lattice.

The relaxation volume of a charged vacancy has contributions from the local atomic relaxation around the vacant lattice site as well as the delocalized electrons present in the system. For a doubly charged oxygen vacancy the net change in volume is  $\Delta \text{Vol}(V_{\text{O}}^{2+}) = \Delta \text{Vol}(\text{ZrO}_2 + V_{\text{O}}^{2+}) + 2\Delta \text{Vol}(\text{ZrO}_2 + e^-)$ . Here,  $\Delta \text{Vol}(\text{ZrO}_2 + e^-)$  is the change in volume of the  $\text{ZrO}_2$  cell with an extra electron and  $\Delta \text{Vol}(\text{ZrO}_2 + V_{\text{O}}^{2+})$  is the change in volume after incorporating a doubly charged vacancy (cell has an effective charge of  $+2e$ ). This calculation yields  $\Delta \text{Vol}(V_{\text{O}}^{2+}) = 5.51 \text{ \AA}^3$  and  $\Delta \text{Vol}(V_{\text{O}}^{1+}) = 2.17 \text{ \AA}^3$ . The decrease in energy during this relaxation process is 0.09 eV for  $V_{\text{O}}^{2+}$ , 0.32 eV for  $V_{\text{O}}^{1+}$  and 0.41 eV for  $V_{\text{O}}$  (the cost of simultaneously putting electrons in the conduction band is not included). The simulation cell following volume relaxation preserves the cubic symmetry. Thus vacancies tend to stabilize the cubic phase in  $\text{ZrO}_2$ .

The process of vacancy formation (say  $V_o^{2+}$ ) can be described by the following equation :



Physically, this means the atmosphere acts as sink for the oxygen atoms removed from  $ZrO_2$ . The removal of a neutral oxygen atom from the system (leaving behind a neutral  $ZrO_2$  lattice) results in a vacant lattice site. The vacant lattice site can trap electrons to form a neutral vacancy or singly charged vacancy.

Fig. 2(a) and Fig. 2(b) shows the formation energy of oxygen vacancy as a function of Fermi level for the charge states  $V_o$ ,  $V_o^{1+}$ ,  $V_o^{2+}$  at  $T = 0$  K and  $T = 2600$  K. When the Fermi level is near the valence band edge,  $V_o^{2+}$  is the most stable charge state of a vacancy, but at higher Fermi levels neutral charge state ( $V_o$ ) becomes energetically favored. We define  $\epsilon(V_o^{2+}/V_o^{1+})$  as the point at which  $V_o^{2+}$  and  $V_o^{1+}$  have similar values of formation energy. It signifies the transition in thermodynamic stability of doubly charged vacancy to a singly charged vacancy with increase in Fermi energy. Also from Fig. 2(a) and Fig. 2(b) we can see that the thermodynamic transition level<sup>30</sup>  $\epsilon(V_o^{2+}/V_o^{1+})$  is located higher than  $\epsilon(V_o^{1+}/V_o^0)$ . Hence, as in the monoclinic phase, the formation of  $V_o^{1+}$  is not favorable in cubic zirconia at any Fermi level, meaning that the oxygen vacancy is a negative- $U$  defect.<sup>10</sup> The defect levels we find are similar to previous estimates using screened exchange method and weighted density approximation.<sup>12</sup>

### 3C. Oxygen Interstitial

Cubic  $ZrO_2$  has  $CaF_2$  structure with metal atoms in a face centered cubic sub-lattice and oxygen atoms occupying a simple cubic sub-lattice. Since the oxygen sub-lattice is not close packed, oxygen defects, rather than zirconium defects, play a dominant role in determining the properties of this oxide. We find that oxygen interstitials in cubic zirconia have different possible atomic structures than those previous reported for the monoclinic phase. We have studied different oxygen interstitial configurations and geometries : (i)  $\langle 110 \rangle$  dumbbell (Fig. 3(a)), (ii)  $\langle 100 \rangle$  dumbbell (Fig. 3(b)), (iii)  $\langle 100 \rangle$  crowd-ion (Fig. 3(c)) and (iv) octahedral site (Fig. 3(d)). For ease of reference the interstitial configurations are labeled as  $O_{\langle 110 \rangle}$ ,  $O_{\langle 100 \rangle}$  respectively for the  $\langle 110 \rangle$ , and  $\langle 100 \rangle$  dumbbell configurations,  $O_{\langle 100c \rangle}$  for  $\langle 100 \rangle$  crowd-ion and  $O_{\text{oct}}$  for octahedral site. Another possible interstitial configuration is  $\langle 111 \rangle$  dumbbell. While  $\langle 110 \rangle$  dumbbell and  $\langle 100 \rangle$  dumbbell have dumbbell centers on an original atomic site, a  $\langle 111 \rangle$  dumbbell configuration upon relaxation

has dumbbell center shifted and not on an original atomic site.  $\langle 111 \rangle$  dumbbell in fact looks quite similar to  $O_{\text{oct}}$ , but not equivalent. It has 0.88 eV higher energy than  $O_{\langle 110 \rangle}$  and the dumbbell separation is  $1.43 \text{ \AA}^3$ .

The relative stability of different interstitial configurations with respect to  $O_{\langle 110 \rangle}$  is compared in Table I. For an oxygen interstitial with neutral charge,  $O_{\langle 110 \rangle}$  configuration is energetically most favorable. The dumbbell separation is close to the O-O bond length in peroxides.<sup>31,32</sup> Incorporation of an extra oxygen atom results in outward movement of the nearest neighbor Zr ions. In this case the lattice distortion is symmetrical about (110) plane. The Zr ions along  $\langle 110 \rangle$  moves 6% (of the Zr-O bond length in an ideal crystal) outward. The nearest neighbor oxygen ions move slightly inward by 0.7%. The two oxygen ions forming the dumbbell structure are separated by  $1.46 \text{ \AA}$ . The change in volume of supercell for  $O_{\langle 110 \rangle}$  was calculated by allowing the supercell to relax. For  $O_{\langle 110 \rangle}$  structure, we find it to be  $36.10 \text{ \AA}^3$ , much higher than the values obtained for vacancies. Volume relaxation destroys the cubic symmetry of the simulation cell.

The electronic local density of states plots near one of the dumbbell ions are the same for spin up and spin down. This is also true for any oxygen atom in the bulk far away from the interstitial configuration. Thus the oxygen ions in the system do not have residual spins. Robertson et al. performed calculations for oxygen interstitials in cubic zirconia and reported electronic properties of  $O_{\langle 100 \rangle}$ , though our findings suggest the  $O_{\langle 110 \rangle}$  as the most stable.

In order to verify the lowest energy configuration we perform ab-initio molecular dynamics (MD) simulations at  $T = 2000 \text{ K}$  for 1.5 ps. The high temperature enhances mobility of the ions and the structures obtained are much different from those at  $T = 0 \text{ K}$ . Next, we select a few intermediate configurations from the MD simulation results and cool them to  $T = 0 \text{ K}$  in molecular dynamics and perform static energy minimization. This procedure typically yields significantly lower-energy structures ( $\Delta E \sim 0.5 \text{ eV}$ ) for vacancies and interstitials. These low energy structures have low symmetry (due to Jahn-Teller distortion). This methodology is well-behaved in that when the same procedure is applied to a perfect cubic zirconia cell, the perfect cell is recovered. When performing this procedure on defects we do not allow the cell lattice vectors to relax, since if this is allowed the cell can become tetragonal.

For singly charged interstitials, we find that the  $O_{\langle 110 \rangle}^{1-}$  configuration is energetically most favorable in contrast to  $O_{\text{oct}}^{1-}$  reported previously by Robertson et al.<sup>12</sup> We come to this conclusion by performing MD simulations at  $T = 2000 \text{ K}$  and then quenching to  $T = 0 \text{ K}$ . After static relaxation, we find the separation between the ions in a dumbbell is  $1.98 \text{ \AA}$ , much higher than that in a

Defect	Interstitial	O <sub>&lt;110&gt;</sub>	O <sub>&lt;111&gt;</sub>	O <sub>&lt;100&gt;</sub>	O <sub>&lt;100c&gt;</sub>	O <sub>oct</sub>
O <sub>i</sub> <sup>0</sup>	Energy (relative, eV)	0	0.88	0.95	1.92	3.02
	Dumbbell separation (Å)	1.46	1.44	1.43	-	-
O <sub>i</sub> <sup>1-</sup>	Energy (relative, eV)	0	-	3.80	3.79	1.90
	Dumbbell separation (Å)	1.98	-	1.93	-	-

TABLE I: Relative stability and dumbbell separations for neutral and singly charged oxygen interstitials in cubic zirconia. After annealing by ab-initio MD and possessing lower symmetry due to Jahn-Teller distortion.

neutral cell. The O<sub><111></sub><sup>1-</sup> configuration becomes unstable and the interstitial atom moves to nearest octahedral site. Table I shows the relative stability of different configurations for a singly charged interstitial with respect to O<sub><110></sub><sup>1-</sup>.

The most stable site for O<sub>i</sub><sup>2-</sup> is the octahedral site. Interstitial atoms placed at the other configurations become unstable and move to occupy the nearest octahedral site upon relaxation. Similar to the neutral oxygen interstitial, the projected density of states for spin-up and spin-down are identical and hence there is no residual spin on the interstitial atom. Similar to the case of charged vacancies, incorporating charged interstitials, O<sub>i</sub><sup>2-</sup> results in large distortion of the parent lattice. The neighboring oxygen and zirconium ions display outward distortions.

Physically, the process of formation of O<sub>i</sub><sup>2-</sup> can be understood by this reaction :



Here, the atmosphere acts as source of oxygen. The system has to be neutral before and after the formation of the interstitial, so formation of a charged interstitial results in the formation of holes. Fig. 2(a) and Fig. 2(b) shows the formation energy of O<sub>i</sub><sup>2-</sup>, O<sub>i</sub><sup>1-</sup> and O<sub>i</sub><sup>0</sup> as a function of the Fermi energy of the system at 1 atm pressure and  $T = 0$  K and  $T = 2600$  K respectively. With increasing temperature incorporation of oxygen interstitials become energetically expensive. For example, the incorporation of neutral interstitial at  $T = 0$  K costs  $E = 0.86$  eV but at  $T = 2600$  K is  $E = 4.12$  eV. From the formation energy plot, we conclude that the thermodynamic defect level  $\epsilon$  (O<sub>i</sub><sup>0</sup>/O<sub>i</sub><sup>1-</sup>) at  $T = 0$  K is higher than  $\epsilon$  (O<sub>i</sub><sup>1-</sup>/O<sub>i</sub><sup>2-</sup>). Hence, as in the monoclinic phase<sup>26</sup>, O<sub>i</sub><sup>1-</sup> is energetically not favored at any Fermi level in cubic ZrO<sub>2</sub>, meaning that the oxygen interstitial is a negative- $U$  defect.

Table II shows some of the possible reactions between the anionic defects in ZrO<sub>2</sub> and their



No.	Reaction	Energy (eV)
1	$O_i^{2-} + O_i^0 \Rightarrow 2O_i^{1-}$	0.83
2	$V_o^{2+} + V_o^0 \Rightarrow 2V_o^{1+}$	0.43
3	$\text{Null} \Rightarrow O_i^0 + V_o^0$	$E_F''=5.15$
4	$\text{Null} \Rightarrow O_i^{1-} + V_o^{1+}$	$E_F'=4.08$
5	$\text{Null} \Rightarrow O_i^{2-} + V_o^{2+}$	$E_F=1.75$
6	$O_i^0 + V_o^0 \Rightarrow O_i^{1-} + V_o^{1+}$	-1.07
7	$O_i^{1-} + V_o^{1+} \Rightarrow O_i^{2-} + V_o^{2+}$	-2.33
8	$O_i^0 + V_o^0 \Rightarrow O_i^{2-} + V_o^{2+}$	-3.40
9	$\text{Null} \Rightarrow e^- + h^+$	$E_g=5.4$

TABLE II: Defect reactions and the corresponding energy change at  $T = 0$  K. The energy change is obtained from the formation energy of the defects. The values reported have been corrected for dipole interactions.

reaction energies. These reaction energies are calculated at 0 K and zero pressure assuming dilute concentration of the defect species. A positive energy means the forward reaction is unfavorable. Reactions 1 and 2 have positive reaction energies, which means that the formation of singly charged interstitials and vacancies are not favored. Thus, two singly charged interstitials or vacancies would decay into neutral and doubly charged defects. Reactions 6-8 suggest that a pair of neutral vacancy and interstitial would prefer to form a pair of doubly charged Frenkel defect.

Next we study the incorporation of an oxygen molecule. The formation energy of an oxygen molecule in cubic  $ZrO_2$  is 10.42 eV at 1 atm oxygen partial pressure and  $T = 2600$  K. At zero pressure and  $T = 0$  K the formation energy is 4.51 eV, much higher than interstitial formation energy of 0.86 eV in a neutral cell. The oxygen molecule formation energy in cubic  $ZrO_2$  is close to the values reported for low temperature monoclinic phase of  $HfO_2$  and much higher than those reported to silica.<sup>33</sup> The bond length of the oxygen molecule is 1.27 Å. By performing MD simulations at 2600K for 1ps and then subsequent relaxation, we find that the molecule prefers to dissociate into two  $\langle 110 \rangle$  dumbbells. The corresponding decrease in energy obtained from static relaxation is 1.93 eV.

#### 4. Defect Equilibrium Reactions

The thermodynamic stability of different point defects can be understood by writing down the equilibrium chemical reactions for the formation of these defects. Analysis of the defect chemistry is done by obtaining the laws of mass action for different competing processes.<sup>34-36</sup> Apart from the laws of mass action, the various point defects present must also satisfy the electronic charge neutrality condition. Here we consider the stable anionic defects in  $ZrO_2$ , namely  $O_i$ ,  $O_i^{2-}$ ,  $V_o$  and  $V_o^{2+}$ . Each defect is considered to be in its lowest energy configuration. In cubic  $ZrO_2$ , the metal ions occupy the closed packed face centered lattice sites. So cationic defect formation energies are much higher than anionic defect formation energies.<sup>37</sup> Hence we neglect the cationic defect contributions in subsequent analysis.

Possible reactions involving  $O_i^{2-}$  and  $V_o^{2+}$  are as follows:

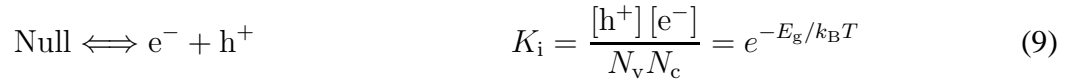
- formation of Frankel defects in the anionic sub-lattice :



- formation of an oxygen vacancy by losing oxygen to the atmosphere :



- formation of electron-hole pair :



- formation of oxygen interstitial :



- and charge neutrality condition :

$$2[O_i]^{2-} + [e^-] = 2[V_o]^{2+} + [h^+] \quad (11)$$

where,  $[e^-]$  and  $[h^+]$  are the electron and hole concentration, respectively,  $[O_i^{2-}]$  is the oxygen interstitial concentration,  $[V_o^{2+}]$  is the oxygen vacancy concentration,  $N_a$  is the concentration of anionic sites and  $E_g$  is the band gap.  $N_c = 2(2\pi m_e^* k_B T / h^2)^{3/2}$  and  $N_v = 2(2\pi m_h^* k_B T / h^2)^{3/2}$  are the constants used to normalize the electron and hole concentration.<sup>36</sup>

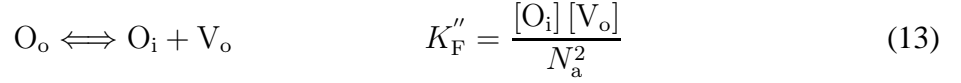
Since  $K_F = e^{-E_F/k_B T}$  and  $K_i = e^{-E_g/k_B T}$ , using values from Table II, we find  $K_F \gg K_i$ . Hence the concentration of electronic defects  $[h^+]$ ,  $[e^-]$  are much smaller than the doubly charged Frankel defects. In this limit, at intermediate oxygen partial pressure, the charge neutrality equation can be simplified (Brouwer approximation<sup>38</sup>) to  $[O_i^{2-}] = [V_o^{2+}] \propto \sqrt{K_F}$ . When the oxygen partial pressure is very high, (10) shifts towards right and we get more oxygen interstitials. So using the charge neutrality (11) condition, the concentration of oxygen interstitials can be expressed in terms of the oxygen partial pressure:

$$[V_o^{2+}] \propto P_{O_2}^{-1/6} \quad [O_i^{2-}] \propto P_{O_2}^{1/6}. \quad (12)$$

The defect concentrations are dependent on multiple factors. In nature, the defect concentrations can be changed by adding dopant or by varying the external environment (temperature and pressure). Here we take undoped zirconia and assume that the defect concentrations, are determined by these two external degrees of freedom.

For the neutral defects the thermodynamic equilibrium reactions for  $O_i$  and  $V_o$  are given by,

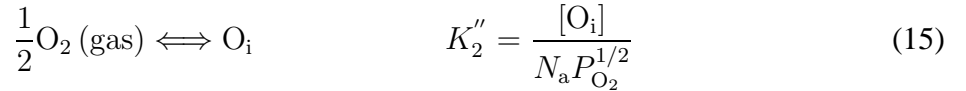
- formation of Frankel defects in the anionic sub-lattice :



- formation of an oxygen vacancy by loosing oxygen to the atmosphere :



- formation of oxygen interstitial :



Analyzing the system for neutral defects is much simpler than the charged defects. Solving the above we get

$$[O_i] \propto P_{O_2}^{1/2} \quad [V_o] \propto P_{O_2}^{-1/2} \quad (16)$$

## 5. Determination of equilibrium Fermi energy

The formation energy plots provide information about the stability of different point defects as a function of temperature, pressure and Fermi energy of the system. Consider for example, defect

formation energies at 2600 K and 1 atm (Fig. 2(b)). The doubly charged defects have the lowest energies. However, for Fermi energy values less than  $\sim 2.1$  eV and more than 3 eV the system becomes unstable leading to spontaneous formation of defects. This pins the Fermi energy of the system to a small region of 2.1 to 3 eV. The overall system needs to maintain charge neutrality. For this to happen the Fermi energy ( $\mu_e$ ) of the system needs to be 2.6 eV so that doubly charged anionic defects have same concentration.

In order to understand this better let us look at the charge neutrality condition for undoped  $\text{ZrO}_2$  described in (11). We neglect the singly charged defects as they are thermodynamically not stable. We do not include the cationic defects as higher formation energy would make their concentration insignificant. As discussed in before, we can have three regimes : (a)  $[e^-] = 2[V_o]^{2+}$  - this implies significant electronic conductivity which is not physical for an insulator like  $\text{ZrO}_2$ ; (b)  $[h^+] = 2[O_i]^{2-}$  - similar to the above condition this is not possible; (c)  $[O_i]^{2-} = [V_o]^{2+}$  - this regime seems physically plausible.

In order to confirm this conclusion, we plot the defect concentrations at 2600 K and 1 atm pressure as a function of the Fermi energy. Fig. 5 shows a comparison between the defect concentrations and the electron and hole concentrations. The defect concentrations are calculated from the rate constants derived from the laws of mass action, namely, (8) and (10). The electron and hole concentrations are obtained by  $[e^-] = N_c e^{-(E_c - \mu)/k_B T}$  and  $[h^+] = N_v e^{-(\mu - E_v)/k_B T}$ . Clearly, the doubly charged defects have much higher concentration than the neutral and singly charged defects. As discussed above, this analysis shows that the electron and hole concentrations are much smaller than the anionic defect concentrations and hence conductivity is by migration of ions.

## 6. Conclusions

An ab-initio study of anionic point defects in cubic zirconia are reported. For  $O_i$  and  $O_i^{1-}$  the energetically favorable configuration is  $\langle 110 \rangle$  dumbbell and for  $O_i^{2-}$  it is an octahedral site. Using a combination of high temperature molecular dynamics and static minimization we obtain the global minima of the potential energy for these defects. Our ground state configurations differ substantially from those previously reported by Robertson et al.<sup>12</sup>

Oxygen interstitials and vacancies in the cubic phase exhibit negative- $U$  behavior, meaning that the singly charged defects are suppressed at any Fermi level. From the analysis of possible reactions between these anionic defects we find that singly charged defect species are thermo-

dynamically less preferable than a combination of neutral and doubly charged defects. Using molecular  $O_2$  as the reference state, defect formation energies are obtained at 0 K and 2600 K. The neutral interstitials have  $\sim 2$  eV higher formation energy than the vacancies at 2600K and 1 atm pressure. The system can lower its energy if the oxygen ions forming the interstitial dumbbell diffuse to the surface and move out to the atmosphere as neutral oxygen molecule. This results in the formation of a neutral vacancy. The corresponding change in energy is  $\Delta E = E(ZrO_2+V_o) - [E(ZrO_2+O_i) - E(O_2)] = -2.49$  eV. Hence, we conclude that neutral interstitials are not stable in cubic zirconia.

We find the relaxation volumes for the anionic vacancies are much smaller than the oxygen interstitials. Unlike the oxygen interstitials, the local atomic relaxation around oxygen vacancies tend to stabilize the cubic phase. We find a charged vacancy has considerably higher relaxation volume compared to a neutral vacancy. Higher relaxation volume signifies that  $ZrO_2$  is susceptible to diffusional creep, which can degrade its mechanical properties with increase in temperature.

Zirconium based materials are attractive for nuclear waste disposal. The Zr-O binary phase diagram<sup>39</sup> shows the existence of non-stoichiometric  $ZrO_{2-\delta}$  phase suggesting vacancies are dominant defect species. Assuming vacancies are dominant defects, we find that change in volume ( $\Delta V$ ) due to presence of defects in cubic  $ZrO_2$  is not large ( $\Delta V/V < 0.5\%$ ). Similar results have also been obtained for  $ZrSiO_4$ .<sup>40</sup>

For a stable system, formation energy of a defect has to be positive. This puts a constrain on the accessible Fermi energy values. From Fig. 2 we see that at 0 K, the feasible Fermi energy values are  $\sim 0.5-1.5$  eV, while at 2600 K Fermi energy of the system lies in the range of  $\sim 2.1-3.0$  eV. For undoped  $ZrO_2$ , the Fermi energy would lie mid-gap, however, the Fermi energy values at low temperature suggest that concentration of doubly charged defects can be tuned by doping with acceptor impurities.

Equilibrium defect concentrations in undoped  $ZrO_2$  are obtained as a function of oxygen partial pressure and temperature by solving the laws of mass action. Based on the charge neutrality condition a method to calculate the Fermi energy of the system is proposed. It is important to note that these defect concentrations are evaluated without accounting for defect interactions. Thus, in the high concentration limit, the actual concentrations can be different from those shown in the figure.

Our results are also relevant to cubic stabilized zirconia (CBZ), in which a p-type dopant such as Y or Ca lower the Fermi level. These low values of Fermi level signifies the abundance of dou-

bly charged oxygen vacancies. Thus, our results demonstrate that, by solving defect equilibrium equation separately and then comparing their concentrations, an estimate of the dominant defect species can be made.

### Acknowledgments

We acknowledge support by the Ohio Supercomputer Center and AFOSR. T. Lenosky wishes to thank Paul Erhart for sharing with him a preprint on point defects in BaTiO<sub>3</sub> prior to publication. A. Samanta wishes to thank Ji Feng for his comments.

---

\* Electronic address: [asamanta@princeton.edu](mailto:asamanta@princeton.edu)

- <sup>1</sup> X. Y. Zhao and D. Vanderbilt, *Physical Review B* **65**, 075105 (2002).
- <sup>2</sup> G. Stapper, M. Bernasconi, N. Nicoloso, and M. Parrinello, *Physical Review B* **59**, 797 (1999).
- <sup>3</sup> A. Bogicevic and C. Wolverton, *Physical Review B* **67**, 024106 (2003).
- <sup>4</sup> W. J. Fleming, *Journal Of The Electrochemical Society* **124**, 21 (1977).
- <sup>5</sup> N. Docquier and S. Candel, *Progress In Energy And Combustion Science* **28**, 107 (2002).
- <sup>6</sup> A. Eichler, *Physical Review B* **64**, 174103 (2001).
- <sup>7</sup> M. M. Opeka, I. G. Talmy, and J. A. Zaykoski, *Journal Of Materials Science* **39**, 5887 (2004).
- <sup>8</sup> F. Monteverde and A. Bellosi, *Journal Of The Electrochemical Society* **150**, B552 (2003).
- <sup>9</sup> A. Bongiorno, C. J. Forst, R. K. Kalia, J. Li, J. Marschall, A. Nakano, M. M. Opeka, I. G. Talmy, P. Vashishta, and S. Yip, *MRS Bulletin* **31**, 410 (2006).
- <sup>10</sup> A. S. Foster, V. B. Sulimov, F. L. Gejo, A. L. Shluger, and R. M. Nieminen, *Physical Review B* **64**, 224108 (2001).
- <sup>11</sup> V. Fiorentini and G. Gulleri, *Physical Review Letters* **89**, 266101 (2002).
- <sup>12</sup> J. Robertson, K. Xiong, and B. Falabretti, *Ieee Transactions On Device And Materials Reliability* **5**, 84 (2005).
- <sup>13</sup> R. I. Grynszpan, G. Brauer, W. Anwand, L. Malaquin, S. Saud, I. Vickridge, and E. Briand, *Nuclear Instruments & Methods In Physics Research Section B-Beam Interactions With Materials And Atoms* **261**, 888 (2007).
- <sup>14</sup> L. Thome, A. Gentils, J. Jagielski, F. Garrido, and T. Thome, *Vacuum* **81**, 1264 (2007).

- 15 L. Thome, A. Gentils, J. Jagielski, F. Garrido, and T. Thome, Nuclear Instruments & Methods In Physics Research Section B-Beam Interactions With Materials And Atoms **250**, 106 (2006).
- 16 C. Degueudre and C. Hellwig, Journal Of Nuclear Materials **320**, 96 (2003).
- 17 G. Kresse and J. Furthmuller, Physical Review B **54**, 11169 (1996).
- 18 G. Kresse and J. Furthmuller, Computational Materials Science **6**, 15 (1996).
- 19 G. Kresse and D. Joubert, Physical Review B **59**, 1758 (1999).
- 20 J. P. Perdew, K. Burke, and M. Ernzerhof, Physical Review Letters **77**, 3865 (1996).
- 21 G. Jomard, T. Petit, A. Pasturel, L. Magaud, G. Kresse, and J. Hafner, Physical Review B **59**, 4044 (1999).
- 22 J. H., G.-A. R. I., R. P., and S. M, Physical Review B **81**, 085119 (2010).
- 23 G. Makov and M. C. Payne, Physical Review B **51**, 4014 (1995).
- 24 D. A. McQuarrie, Statistical Mechanics, Harper Collins Publishers (1976).
- 25 D. S. Villars, Proceedings of the National Academy of Sciences **15**, 705 (1929).
- 26 A. S. Foster, A. L. Shluger, and R. M. Nieminen, Physical Review Letters **89**, 225901 (2002).
- 27 B. Kralik, E. K. Chang, and S. G. Louie, Physical Review B **57**, 7027 (1998).
- 28 S. Fabris, A. T. Paxton, and M. W. Finnis, Acta Materialia **50**, 005171 (2002).
- 29 F. A. Kroger and H. J. Vink, Solid State Physics - Advances in Research and Applications, Academic Press, New York (1957).
- 30 P. E. Blochl and H. Stathis, Physical Review Letters **83**, 372 (1999).
- 31 S. X. Tian, Journal Of Physical Chemistry B **108**, 20388 (2004).
- 32 V. I. Avdeev, S. F. Ruzankin, and G. M. Zhidomirov, Journal Of Structural Chemistry **38**, 519 (1997).
- 33 A. S. Foster, F. L. Gejo, A. L. Shluger, and R. M. Nieminen, Physical Review B **65**, 174117 (2002).
- 34 R. A. Huggins, Solid State Ionics **143**, 3 (2001).
- 35 K. P. Bogdanov, D. T. Dimitrov, O. F. Lutskaya, and Y. M. Tairov, Semiconductors **32**, 1033 (1998).
- 36 M. W. Barsoum, Fundamentals of ceramics, Institute of Physics Publishing (1997).
- 37 J. X. Zheng, G. Ceder, T. Maxisch, W. K. Chim, and W. K. Choi, Physical Review B **75**, 104112 (2007).
- 38 G. Brouwer, Philips Research Reports **9**, 366 (1954).
- 39 R. J. Ackermann, S. P. Garg, and E. G. Rauh, Journal of The American Ceramic Society **60**, 341 (1977).
- 40 J. M. Pruneda, T. D. Archer, and E. Artacho, Physical Review B **70**, 104111 (2004).

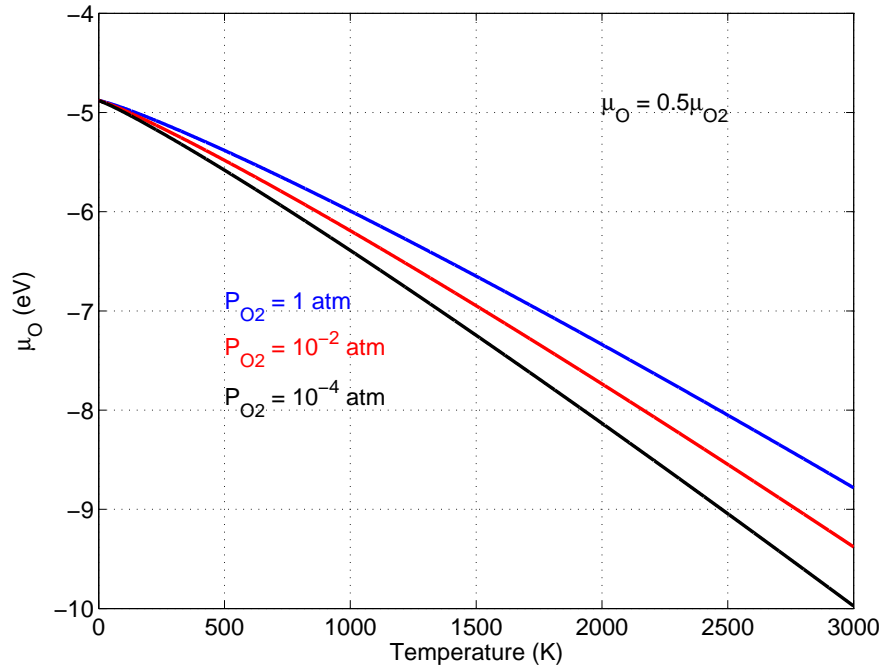
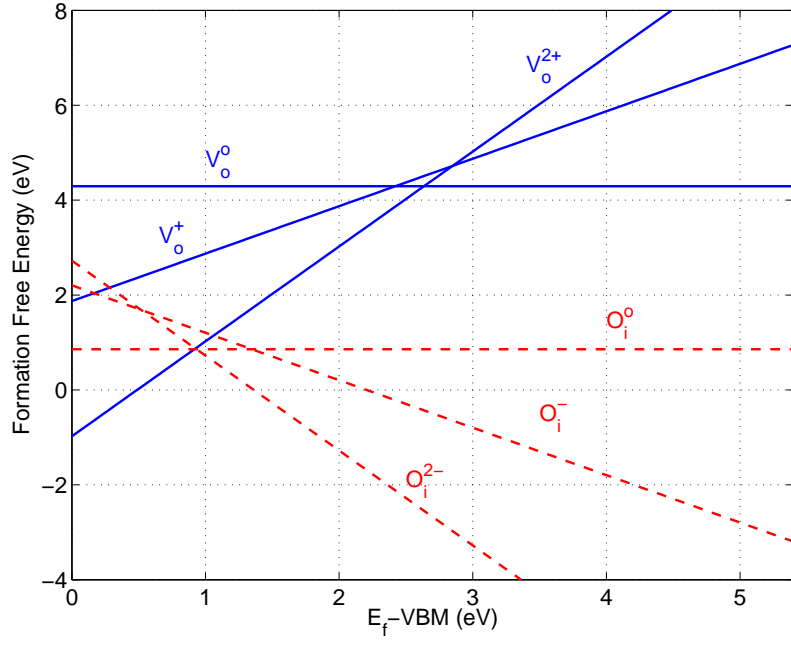
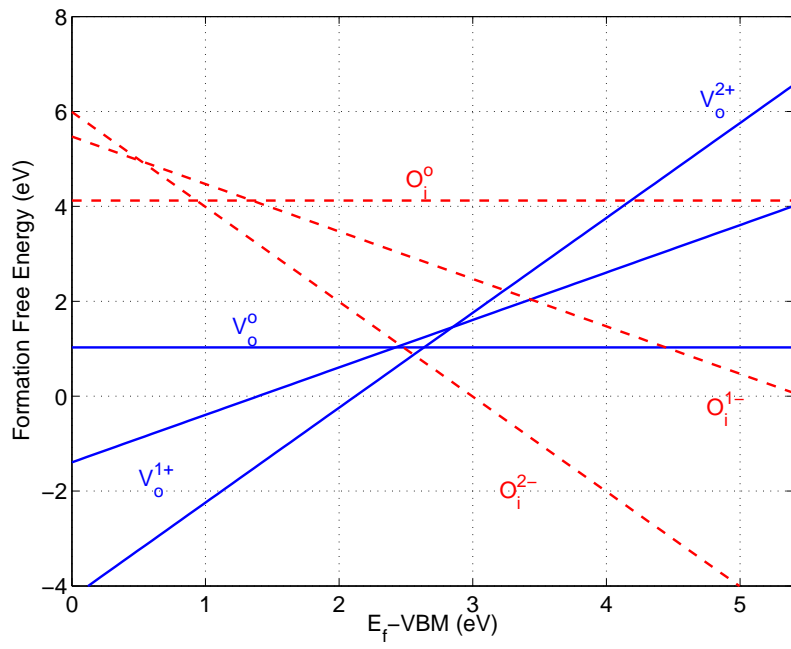


FIG. 1: The chemical potential of an oxygen atom as a function of temperature at different oxygen partial pressures calculated from the quantum formulation of an ideal gas. ( $\mu_{\text{O}} = 0.5\mu_{\text{O}_2}$ )





(a)



(b)

FIG. 2: Formation energy of point defects in cubic ZrO<sub>2</sub> as function of the Fermi energy at 2(a)  $T = 0$  K and 2(b)  $T = 2600$  K and 1 atm.

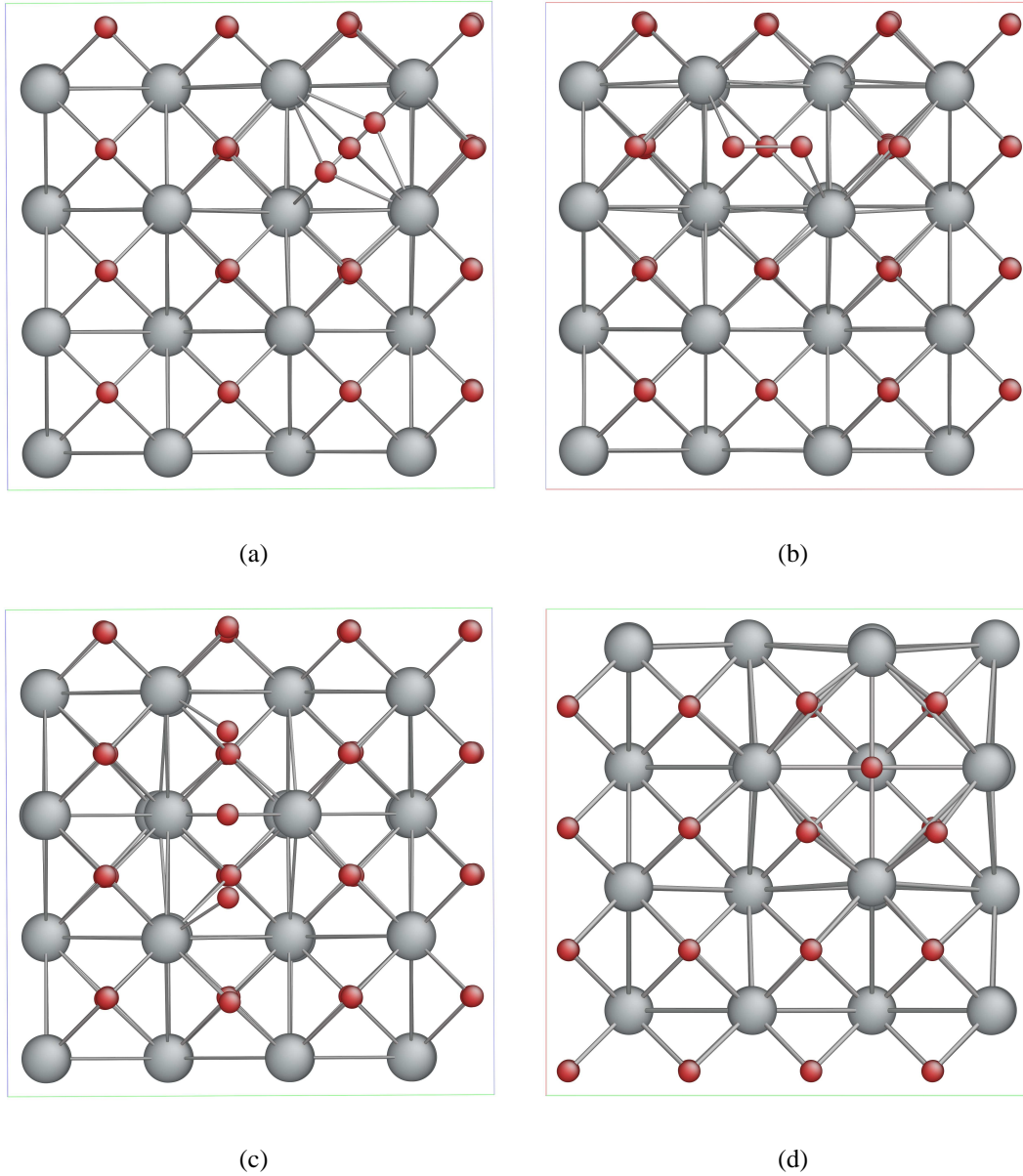


FIG. 3: Snapshots of oxygen interstitial configurations in cubic zirconia viewed along  $(100)$  direction. 3(a) The  $\langle 110 \rangle$  dumb bell configuration neutral oxygen interstitial. This is the lowest energy configuration of the neutral oxygen interstitial, which is energetically favored at low Fermi level. 3(b)  $\langle 100 \rangle$  crowdion configurations of neutral oxygen interstitial. 3(c)  $\langle 100 \rangle$  crowdion configurations of neutral oxygen interstitial. 3(d) Doubly charged oxygen interstitial in octahedral configuration. This is the ground state of a doubly charged oxygen interstitial.

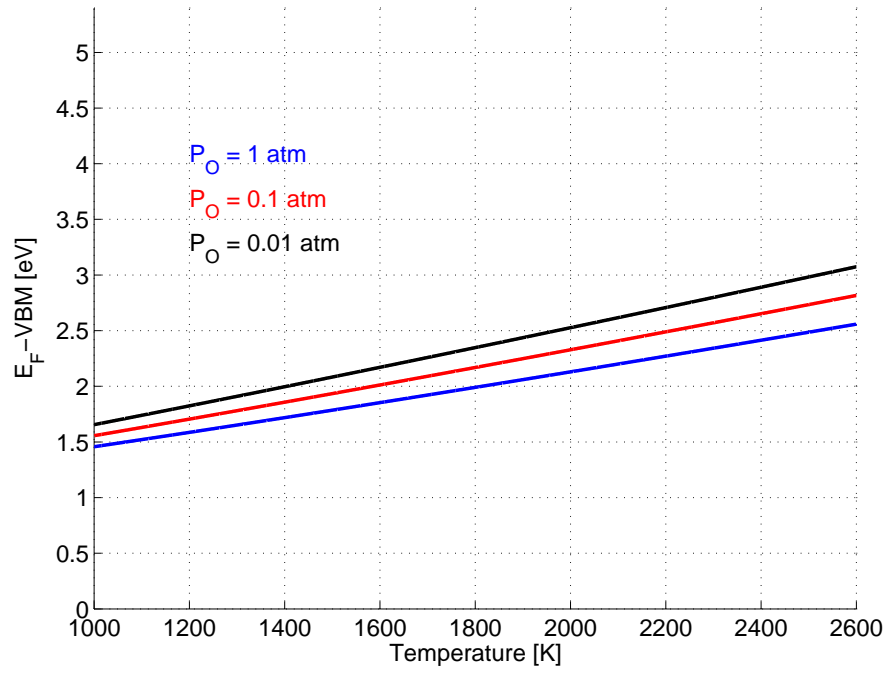


FIG. 4: The chemical potential (Fermi energy) of an undoped cubic  $ZrO_2$  system as a function of temperature at different oxygen partial pressures.

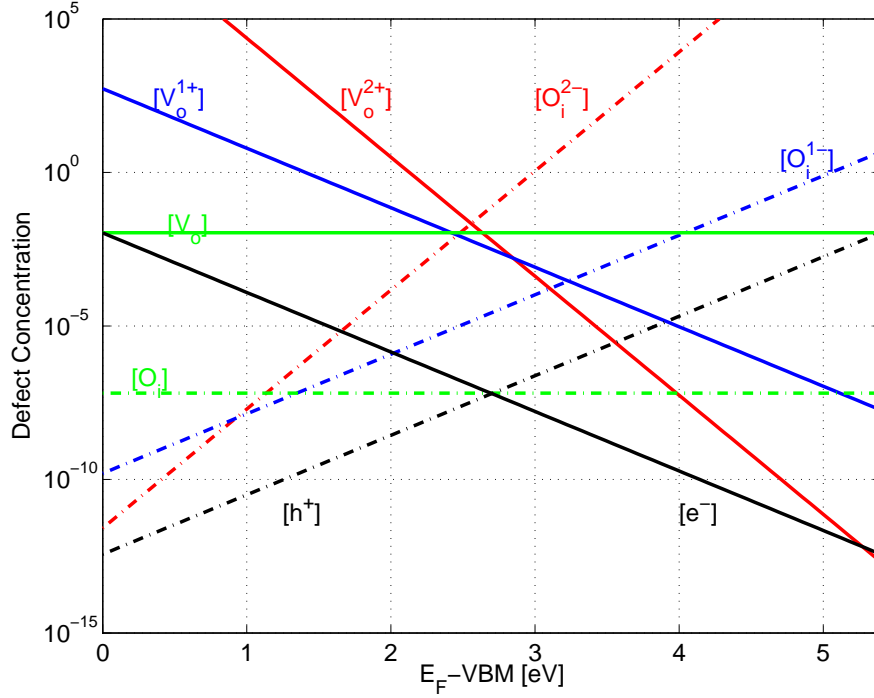


FIG. 5: Comparison of point defect concentration as a function of Fermi level of the system at 1 atm pressure and  $5 T = 2600$  K. The concentration profiles are obtained by solving each set of defect equilibrium equations separately. The doubly charged defects :  $V_o^{2+}$  (solid red line) and  $O_i^{2-}$  (dotted red line) have higher concentration than the singly charged ( $V_o^{1+}$  - solid blue line, and  $O_i^{1-}$  - dotted blue line) and neutral defects ( $V_o$ ) - solid green line, and  $O_i$  - dotted green line. The defect concentrations are expressed as fraction of anionic sites in the system.